InGaAs/AlGaAsSb avalanche photodiodes with sub 100 fW/√Hz noise equivlent power at 22 to 52 °C

Longyan Li*
School of Electrical and Electronic Engineering
University of Sheffield
Sheffield, UK
lli52@sheffield.ac.uk
*Corresponding author

Jonathan D. Petticrew
School of Electrical and Electronic Engineering
University of Sheffield
Sheffield, UK
j.d.petticrew@sheffield.ac.uk

Jonathan Taylor-Mew
School of Electrical and Electronic Engineering
University of Sheffield
Sheffield, UK
j.taylor-mew@sheffield.ac.uk

Jo Shien Ng
School of Electrical and Electronic Engineering
University of Sheffield
Sheffield, UK
j.s.ng@sheffield.ac.uk

Chee Hing Tan
School of Electrical and Electronic Engineering
University of Sheffield
Sheffield, UK
c.h.tan@sheffield.ac.uk

***Abstract*— Separate – Absorption - Multiplication Avalanche Photodiode (SAM-APD) made from $Al_{0.85}Ga_{0.15}As_{0.56}Sb_{0.44}$ (AlGaAsSb) avalanche region and InGaAs absorption region exhibits low dark current, excess noise, and Noise Equivalent Power (NEP) at room temperature. However, its performance at elevated temperatures has not been reported. In this work we performed comprehensive measurements of dark current, avalanche gain and noise spectrum of three InGaAs/AlGaAsSb SAM-APDs at 22 to 52 °C. We observed a weak temperature dependence of dark current and breakdown voltage has a temperature coefficient of 12.9 (± 0.5) mV/°C, which is 6 – 15 times better than a number of commercial 1550 nm APD modules. The best NEP ranges between 78 and 92 fW/√Hz at 22 to 52 °C with NEP at 52 °C outperforming a number of commercial 1550 nm APD modules at 22 °C. The low NEP value enable the InGaAs/AlGaAsSb SAM-APDs to detect optical pulse with as few as 78 photons per pulse at 22 °C, increasing to 100 photons at 52 °C. These results demonstrate that InGaAs/AlGaAsSb SAM-APDs have a superior temperature tolerance to maintain gain, NEP and low photon detection compared to typical 1550 nm SAM-APDs. Therefore, they can potentially increase the range and sensitivity of gas sensing, free space optical communication and ranging instruments.**

Keywords—AlGaAsSb, Avalanche photodiodes (APDs), Infrared detectors, noise equivalent power, Signal-to-noise-ratio

I. INTRODUCTION

Avalanche photodiodes (APDs), operated in either Linear or Geiger mode, are widely used in applications requiring detection of low photon infrared signals, including long range optical networks [1], optical time domain reflectometer [2], light detection and ranging (LiDAR) [3] and remote gas sensing [4]. In optical fibre-based applications, 1310 and 1550 nm wavelengths are used due to low dispersion and low attenuation in standard silica optical fibres. For LiDAR, operating at 1550 nm instead of 905 nm wavelength offers (i) higher limit of optical transmitter power (by ~ 6 orders of magnitude because of eye safety considerations [3]) and (ii) greater penetration through fog. Similarly, 1550 nm is used in commercial free space optical communication (FSOC) systems capable of reaching 30 Gb/s over a link distance up to 1300 m [5] and is the recommended wavelength for the Lunar Optical Communications [6]. Moreover, the wavelengths around 1570 and 1645 nm are used in remote sensing of important gases (such as carbon dioxide (CO_2) [7] and methane (CH_4) [4], respectively) due to the strong gas absorption peaks.

Noise Equivalent Power (NEP), defined as the minimum optical power required to achieve a unity SNR, is often used to describe performance of optical receivers. In both LiDAR and FSOC, the NEP provides the equivalent optical power level (signal) required to overcome the voltage noise of the output of the photoreceiver amplifier. Therefore, with a low NEP, a longer range and a better signal to noise ratio can be achieved. APDs are used in LiDAR systems because they provide high quantum efficiency, fast response time and high sensitivity. For example, in a study for the baseline configuration of Methane Remote sensing LiDAR Mission (MERLIN) for CH_4 sensing (~1645 nm) uses an InGaAs APD (Laser components, IAG200T6) with a gain of $M = 10$ and an excess noise factor of $F = 3.2$ [8]. It was predicted that this APD can enable a modestly sized LiDAR instrument on a 506 km orbit to provide a 50 km averaged methane column measurement. Likewise, high sensitivity APDs are utilised in FSOC for high bit rate optical backhaul downlinks. For example, the CAPANINA project [9] achieved a bit rate up of 1.25 Gb/s at 1550 nm wavelength over a 22 km range with optical signal as weak as 168 photons per bit [10].

The gain and excess noise factor are key parameters in the NEP, which is given by $\text{NEP} = \frac{1}{RM}\sqrt{2qI_dM^2F + i_{amp}^2}$, where R is the APD's responsivity at unity gain, q is the electron charge, I_d is the APD bulk dark current, and i^2_{amp} is the current noise of the optical receiver's electronic amplifier. To minimize NEP, we need to minimize I_d and F while maximizing M and R. Since the APD's dark current usually increases with temperature, achieving a low NEP at elevated temperatures can be challenging. This is particularly relevant in automotive

This work was supported by the UK Engineering and Physical Sciences Research Council and Phlux Technology Ltd., EP/Y024745/1 - SPARC; and the Centre for Earth Observation Instrumentation, RP16W506420A03.

LiDAR, where discrete semiconductor devices need to operate above room temperature [11]. Therefore, it is desirable to have an APD that can achieve low NEP at and above room temperature, which is a key focus of this work.

APDs detecting light at 1550 - 1650 nm typically adopt a separate absorption and multiplication (SAM) structure, utilizing a narrow bandgap material such as $In_{0.53}Ga_{0.47}As$ (lattice-matched to InP, hereafter InGaAs) for efficient photon absorption and a wide bandgap material such as InP or $In_{0.52}Al_{0.48}As$ (hereafter, InAlAs) as the avalanche material. At M = 10, InP and InAlAs typically exhibit F ~ 3.5 [12] and ~ 3.1 [13], respectively. The high F values limit the NEP to 110 – 160 fW/√Hz in commercial InGaAs APD modules [14], [15], [16]. To improve the NEP, an alternative avalanche material with low F can be used. $Al_{0.85}Ga_{0.15}As_{0.56}Sb_{0.44}$ (lattice-matched to InP, hereafter AlGaAsSb) exhibits very low excess noise factors (F < 2 at M = 25) [17] due to a large ratio of electron to hole ionization coefficients [18]. AlGaAsSb avalanche regions were combined successfully with InGaAs [19] and GaAsSb [20] absorption regions to form SAM-APDs. Recently InGaAs/AlGaAsSb SAM APD receiver exhibiting excellent $F(M)$ characteristics were reported [21] and a very low room temperature NEP of 46.3 fW/√Hz [22] was achieved. This NEP value is significantly lower than those values in [14], [15], [16], demonstrating the potential of improving LiDAR and FSOC systems using InGaAs/AlGaAsSb APDs.

In addition to low NEP, the breakdown voltages, V_{bd}, of AlGaAsSb based SAM-APDs are relatively stable with temperature. Their experimental values of temperature coefficient of breakdown voltage, C_{bd}, are 13.5 [23], 4.31 (derived from 77 to 295 K data) [24], and 11.83 mV/K (derived from 296 to 353 K data) [25]. These are much lower than typical C_{bd} values from other commercial APDs for 1550 - 1650 nm wavelength (~100 mV/K) [26]. An APD with a low C_{bd} will show temperature-stable avalanche gain too. For instance, the avalanche gain of a homojunction AlGaAsSb p-i-n diode varies by only 15 % when temperature increases from 24 to 80 ºC [27], suggesting that AlGaAsSb SAM-APDs could maintain high performance at high temperature. However, NEP values of InGaAs/AlGaAsSb SAM-APDs at elevated temperatures have not been reported. In this work we report the detail characterization of InGaAs/AlGaAsSb SAM-APDs at elevated temperatures. The SAM-APDs were evaluated through measurements of dark current, avalanche gain, and NEP at 1550 nm at 22 to 52 °C, allowing performance in detecting low photon infrared signals to be assessed. The data reported in this article is available from ORDA digital repository [28].

II. Experimental Details

The InGaAs/AlGaAsSb SAM-APDs used in this work were acquired from Phlux Technology, Ltd [29]. The details of the epitaxial layers and the device fabrication procedures are not available to us. Three SAM-APDs (A, B and C) with 200 µm diameter optical aperture, from the Aura Series [29], were used in this work. The APD temperature was maintained at 22 to 52 °C, under vacuum in a variable temperature probe station (Janis Research, model ST-500). The temperature dependent dark current, M, NEP, and low photon measurements were performed on all three APDs at the temperature from 22 to 52 °C.

Reverse bias, V_b for the APD was supplied by a Source-Measure-Unit in all the measurements. For measurements requiring optical signals, a single mode optical fibre coupled 1550 nm wavelength light from a modulated laser (6.5 kHz frequency and 50 % duty cycle) onto the APD's optical window. The APD's current was amplified and converted into a voltage signal using a Stanford Research SR570 low-noise current pre-amplifier at a sensitivity of 10 µA/V with a noise specification of 2 pA/√Hz and a bandwidth of 200 kHz [30]. The pre-amplifier's output voltage was detected using a Fast Fourier Transform (FFT) spectrum analyser, so the modulated photocurrent could be distinguished from the dark current.

The APD's responsivity is quoted as R = 0.98 A/W at 1550 nm in the data sheet [29]. When operated with an internal gain, the multiplied responsivity was given by the ratio of measured photocurrent (obtained from FFT spectrum analyser) to the incident optical power (measured with a commercial optical power meter). To determine gain at higher temperature, we assumed that the responsivity will have a similar temperature-dependence of a commercial InGaAs photodiode with data from - 40 to 60 °C [30]. At 1550 nm the responsivity increases by 0.32 mA/W per ºC, so that $R(T) = 0.98 + 0.32 \times 10^{-3}$ A/W. $M(V)$ was obtained from the ratio of the multiplied responsivity to APD's responsivity at the fixed temperature. The breakdown voltage, V_{bd}, was determined by linear regression fitting to $1/M(V)$ data extract the bias corresponding to $1/M(V) = 0$.

The spectrum analyser was also used to measure the noise power spectral density (PSD), V_{noise}, to yield NEP, expressed as,

$$NEP = \frac{V_{noise} \times S_{amp}}{R \times M}, \quad (1)$$

where S_{amp} is the sensitivity of the pre-amplifier. The measurements were centred on the laser modulation frequency with a 97.5 Hz frequency span and a 244 mHz linewidth. Each spectra was obtained by averaging across 1000 measurements.

To assess the minimum photon detection, the laser power was attenuated to the lowest level while ensuring the signal is clearly above the noise floor. We have ensured all measurements exhibits a SNR between 3 and 4. The attenuation was achieved using a -25 dB fixed attenuator and a variable attenuator (0 to - 80 dB). The number of photons per optical pulse was given by $n_{photon} = \tau P_{peak}/E$, where P_{peak} is the peak optical power, τ is the laser pulse duration (76.9 µs) and E is the photon energy (0.8 eV).

III. Results and Discussion

The reverse bias dark current characteristics of the three APDs at 22 to 52 °C are shown in Fig. 1 (a). The dark current of APD C is slightly higher than those of A and B. At 22 ºC, the dark current from each APD increases abruptly at 65.6 V, indicating breakdown. As the temperature increases from 22 to 52 °C, there is a small increase in dark current for $V_b < V_{bd}$. At

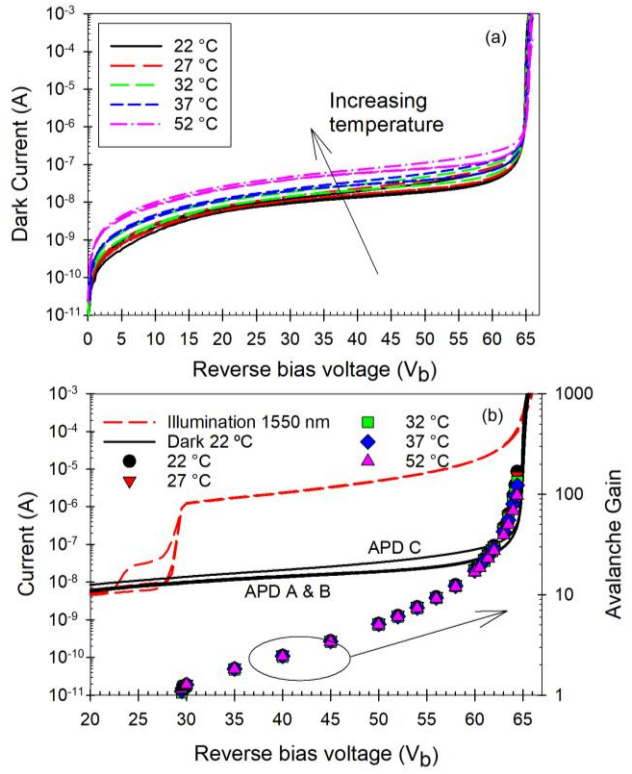

Fig. 1. (a) Dark current characteristics from the three APDs at 22 to 52 °C. (b) Dark current and photocurrent under 1550 nm wavelength illumination at 22 °C (left axis, lines) as well as mean avalanche gain (right axis, symbols) at 22 to 52 °C from the three APDs.

$V_b = 0.9 \times V_{bd}$, the dark current increases by 1.03 times for every 1 ºC rise in temperature.

Under a 1550 nm laser illumination at room temperature, the APD photocurrent increases abruptly at ~ 29.8 V. This was interpreted as the punch-through voltage, as shown in Fig. 1 (b). We observed that one of the APDs has a slight increase in photocurrent at ~ 25 V, prior to the punch-through voltage. At V_b = 29.8 V, the three APDs' responsivity values range from 1.14 to 1.18 A/W at 1550 nm. These values indicated M ~ 1.2 at 29.8 V, since R = 0.98 A/W at M = 1, as stated in the data sheet [29].

The mean value of $M(V)$ from the three APDs are shown in Fig. 1 (b). At 22 ºC, the APDs achieved M > 150 before dark current prevented reliable measurements. For a given V_b, M decreases with increasing temperature, as expected for AlGaAsSb based SAM-APDs [20], [23]. At a fixed V_b corresponding to M = 10 at 22 °C, raising the APD temperature to 52 °C reduces M by 5.7, 3.9 and 3.0 %, for APD A, B and C, respectively. Hence the average reduction of M = 10 from 22 to 52 °C is 4.2 %, with a rate of 0.14 %/°C. Repeating the analysis for M = 20, 30 and 50 produce the temperature dependence shown in Fig. 2 (a). The percentage reduction changes from 0.14 %/°C for M = 10 to 0.60 %/°C for M = 50. Fig. 2 (a) also include values extracted from commercial Si [31], [32], InGaAs/InAlAs [33] and InGaAs/InP [34] SAM-APDs. At M = 10 to 50, the InGaAs/AlGaAsSb SAM-APDs exhibit 3 to 4 times smaller percentage reduction than the InGaAs/InP, InGaAs/InAlAs and Si APDs.

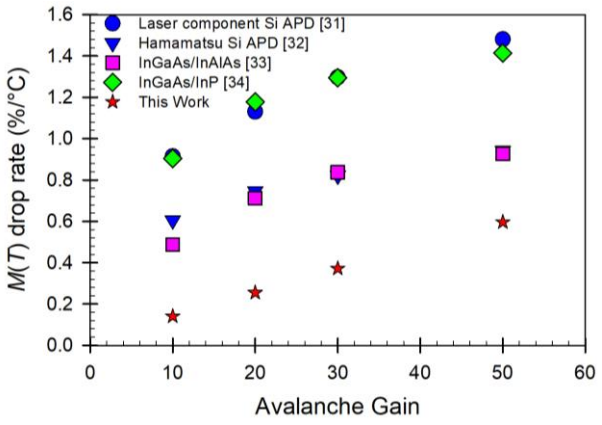

Fig. 2. Temperature dependence of M for above room temperature, where room temperature is 20 to 25 °C depending on datasheet. Mean values from three APDs are reported for this work.

The experimental V_{bd} versus temperature results for the three APDs are shown in Fig. 2. Linear regression fittings yielded C_{bd} of 12.4 - 13.2 mV/ºC, giving a mean value of 12.9 (± 0.5) mV/ºC. This C_{bd} value is 6 - 15 times smaller than those from typical commercial APD-amplifier modules (with InGaAs absorption region), that exhibit C_{bd} values of 80 [14], 100 [16] and 200 mV/ºC [15]. The smaller C_{bd} and lower $M(T)$ reduction in the AlGaAsSb avalanche region may be attributed to alloy scattering, which is a significant carrier scattering mechanism governing AlGaAsSb avalanche statistics [18] (possibly due to very different covalent radii of the Sb and As atoms [35], [36]). Alloy scattering has negligible temperature dependence so its significance in AlGaAsSb may have an desirable effect on temperature stability of AlGaAsSb APDs.

Power density spectra from the NEP measurements using an optical power of ~ 2.6 nW and varying APD V_b are compared in Fig. 3. For clarity, only data from APD B are presented here. As V_b increases, V_{noise} increases slightly at V_b between 30 and 61 V, before a noticeable from 61 to 64 V. From 30 to 64 V, the signal amplitude increases from 3.2×10^{-4} to 5.6×10^{-3} $V_{RMS}/\sqrt{\text{Hz}}$, corresponding to M ~ 1.3 and 23, respectively. Therefore the SNR improves from ~ 2850 at 30 V to ~ 33,500 at 61 V.

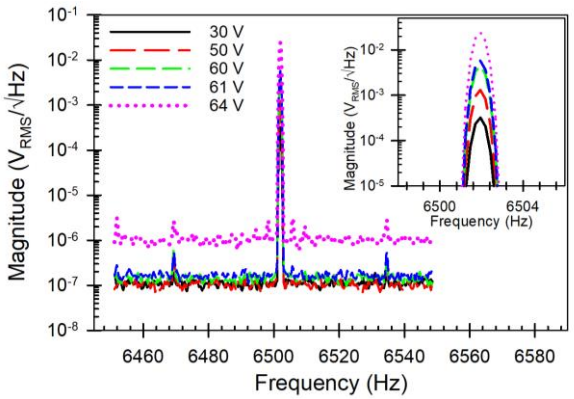

Fig. 3. Measured power density spectra from APD B under varying V_b at 22 °C. Inset shows the signal peaks.

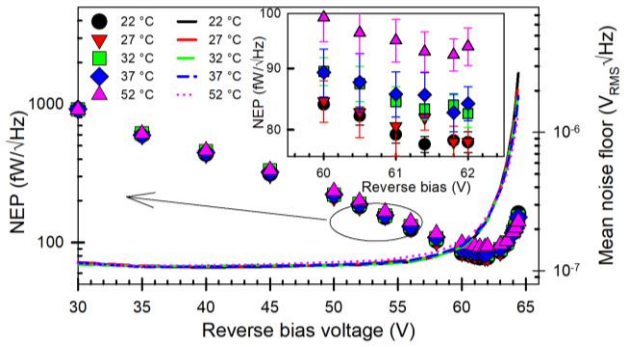

Fig. 4. Mean NEP (left axis, symbols) and noise floor (right axis, lines) versus reverse bias as a function of temperature from three APDs under 1550 nm wavelength illumination. Inset shows the mean NEP data with the standard deviations (as error bars) around reverse bias of 61 V.

The experimental results of noise floor measured as V_{RMS} and NEP from the three APDs at 22 to 52 °C are similar, so only their mean values are shown in Fig. 4, respectively. For a given temperature, The noise floor increases rapidly when V_b > 61 V (M ~ 23), causing the APD noise to dominate over the TIA noise. Consequently, the best (lowest) NEP values are at V_b ~ 62 V. The best NEP value for a given temperature worsens from 78 fW/√Hz at 22 ºC to 92 fW/√Hz at 52 ºC. The best NEP value of 78 fW/√Hz at 22 ºC is slightly larger than the 46.3 fW/√Hz from [22]. The discrepancy may be due to noise floor at V_b above 61 V (possibly caused by parasitic capacitance between the probe station and the pre-amplifier), limiting our optimum gain to M ~ 26 compared to ~ 170 in [22].

Table I compares the NEP values at 1550 nm wavelength from this work with selected commercial APD modules (all with APD diameter of 200 µm) [14], [15], [16]. The InGaAs/AlGaAsSb SAM-APD has the lowest NEP. It is interesting to note that the measured NEP value at 52 ºC is lower than those of the commercial modules at 22 ºC, confirming that superior temperature stability and low noise of the InGaAs/AlGaAsSb SAM-APD at elevated temperatures.

TABLE I. PERFORMANCE COMPARISON WITH COMMERCIAL APD MODULES AT THE WAVELENGTH OF 1550 NM.

Performance parameter	**Commercial APD Modules**			
	CMC Electronics [14]	***Excelitas [15]***	***Analog Modules [16]***	***This work***
APD diameter (µm)	200	200	200	200
C_{bd} (mV/°C)	80	200	100	12.9
NEP @ 22 °C (fW/√Hz)	110 @ 1570 nm	130	160	78
NEP @ 52 °C (fW/√Hz)	---	---	---	92

We have evaluated the minimum number of photons that can be detected by the APDs at 1550 nm. PSD spectra of APD B obtained at V_b ~ 61 V and overall SNR between 3 and 4 are shown as examples of measured data in Fig. 5. As temperature varied between 22 and 52 °C, APD B could detect optical pulses with as few as 75 - 95 photons per pulse. The corresponding values for APD A and C are 71 - 94 and 87 - 111 photons per

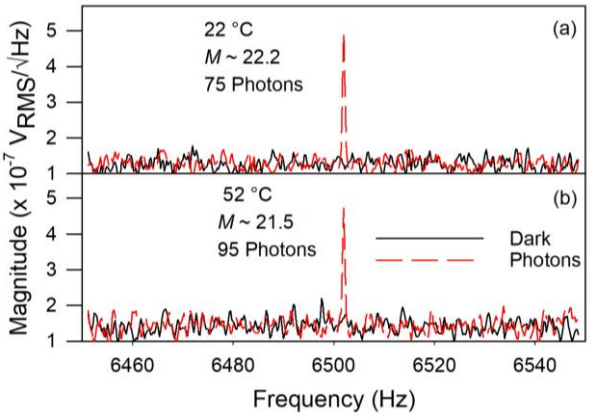

Fig. 5. PSD spectrum at low number of 1550 nm wavelength photons per pulse from APD B at V_b = -61V and at temperature of (a) 22 and (b) 52 °C.

pulse. Thus, the mean values are 78 photons per pulse at 22 ºC and 100 photons per pulse at 52 ºC.

IV. CONCLUSION

Comprehensive InGaAs/AlGaAsSb SAM APD characterization was carried out at 22 to 52 ºC. The three APDs show highly consistent performance with high tolerance to temperature. The dark current increases slowly with temperature at a rate of 1.03 times/ºC. The avalanche gain drops with temperature. The percentage reduction changes from 0.14 %/°C for M = 10 to 0.60 %/°C for M = 50, which is 3 - 4 times smaller than typical commercial InGaAs/InP, InGaAs/InAlAs and Si APDs. This confirms the advantage of the small coefficient of breakdown voltage in InGaAs/AlGaAsSb APD, which was found to be 6 - 15 times smaller than other InGaAs-based APDs. Since the dark current and gain directly impact the NEP, the weak temperature dependence of dark current and gain in AlGaAsSb is desirable. The best NEP values at the 1550 nm wavelength are 76 - 78 fW/√Hz at 22 ºC, increasing slightly to 89 - 96 fW/√Hz at 52 ºC, which is lower than a number of existing commercial APD modules. These low NEP values enabled the InGaAs/AlGaAsSb SAM-APDs to detect optical pulses with as few as 78 and 100 photons at 22 and 52 ºC, respectively. Our experimental results confirm that InGaAs/AlGaAsSb APDs are stable with temperature and offer low noise performance at above room temperature. The InGaAs/AlGaAsSb SAM-APD showed a potential of thermal stabilizer free on elevated temperature range while maintaining the sub-100 photons per pulse detection performanc.

REFERENCES

[1] J. C. Campbell, 'Recent Advances in Telecommunications Avalanche Photodiodes', *J. Light. Technol.*, vol. 25, no. 1, pp. 109–121, Jan. 2007, doi: 10.1109/JLT.2006.888481.

[2] B. F. Levine, C. G. Bethea, and J. C. Campbell, 'Room-temperature 1.3-µm optical time domain reflectometer using a photon counting InGaAs/InP avalanche detector', *Appl. Phys. Lett.*, vol. 46, no. 4, pp. 333–335, Feb. 1985, doi: 10.1063/1.95622.

[3] P. F. McManamon, 'Significant Applications of LiDAR,' in LiDAR Technologies and Systems, Bellingham, Washington, USA: SPIE Press, 2019, ch. 11, pp. 459 – 497.

[4] J. Titchener, D. Millington-Smith, C. Goldsack, G. Harrison, A. Dunning, X. Ai, and M. Reed, 'Single photon Lidar gas imagers for practical and widespread continuous methane monitoring', *Appl. Energy*, vol. 306, Jan. 2022, Art. No. 118086, doi: 10.1016/j.apenergy.2021.118086.

[5] EC System, EL-10Gex datasheet, Accessed: July 13, 2025. [Online]. Available: http://www.ecsystem.cz/en/products/free-space-optic-equipment/free-space-optics-30-gigabits.

[6] B. L. Edwards, , 'Latest Status of the CCSDS Optical Communications Working Group', *254 Proceedings of IEEE International Conference on Space Optical Systems and Applications 255 (ICSOS)*, Mar 28-31. 2022, Kyoto, Japan.

[7] A. Amediek, A. Fix, G. Ehret, J. Caron, and Y. Durand, 'Airborne lidar reflectance measurements at 257 1.57 μm in support of the A-SCOPE mission for atmospheric CO2', *Atmos. Meas. Tech.*, vol. 2, no. 2, pp. 755-772, Nov. 2009, doi: 10.5194/amt-2-755-2009.

[8] C. Kiemle, M. Quatrevalet, G. Ehret, A. Amediek, A. Fix, and M. Wirth, 'Sensitivity studies for a space-based methane lidar mission', *Atmos. Meas. Tech.*, vol 4, no. 10, pp 2195 – 2211, Oct. 2011, doi: 10.5194/amt-4-2195-2011.

[9] D. Giggenbach, J. Horwath, 'Optical Free-Space Communications Downlinks from Stratospheric Platforms – Overview on STROPEX, the Optical Communications Experiment of CAPANINA', in *Proc. 2005 IST Mob. Sum. Conf.*, Dresden, Germany, 2005.

[10] J. Horwath, M. Knapek, B. Epple, M. Brechtelsbauer, and B. Wilkerson, 'Broadband backhaul communication for stratospheric platforms: The stratospheric optical payload experiment (STROPEX)', in *Free-Space Laser Communications VI*, vol. 6304, A. K. Majumdar and C. C. Davis, Eds. Bellingham, WA, USA: SPIE, 2006, pp. 436–447.

[11] *Failure Mechanism Based Street Test Qualification for Discrete Semiconductors (base document)*, AEC-Q101- REV – E, Automotive Electronic Council, U.S.A, Mar. 2021.

[12] L. J. J. Tan, J. S. Ng, C. H. Tan, and J. P. R. David, 'Avalanche Noise Characteristics in Submicron InP Diodes', *IEEE J. Quantum Electron.*, vol. 44, no. 4, pp. 378–382, Apr. 2008, doi: 10.1109/jqe.2007.914771.

[13] Y. L. Goh, A. R. J. Marshall, D. J. Massey, J. S. Ng, C. H. Tan, M. Hopkinson, J. P. R. David, S. K. Jones, C. C. Button, and S. M. Pinches, 'Excess Avalanche Noise in $In_{0.52}Al_{0.48}As$', *IEEE J. Quantum Electron.*, vol. 43, no. 6, pp. 503–507, Jun. 2007, doi: 10.1109/JQE.2007.897900.

[14] *CMC Electronics*, Dual Wavelength InGaAs Avalanche Photodiode Preamplifier Module (264-339822) datasheet, 2022. Accessed: July 13, 2025. [Online]. Available: https://cmcelectronics.ca/wp-content/uploads/2022/09/4.5.2-264-339822-APD-receiver-brochure_web.pdf.

[15] *Excelitas Technologies*, C30659 series datasheet, 2023. Accessed: July 13, 2025. [Online]. Available: https://www.excelitas.com/product/c30659-1550-r2ah-ingaas-apd-receiver-200um-8-50mhz.

[16] *Analog Modules*, High Sensitivity APD Optical Receiver (7511B-1-04) datasheet, 2022". Accessed: July 13, 2025. [Online]. Available: https://analogmodules.com/wp-content/uploads/7511B-1-04.pdf.

[17] J. Taylor-Mew, V. Shulyak, B. White, C. H. Tan, and J. S. Ng, 'Low Excess Noise of $Al_{0.85}Ga_{0.15}As_{0.56}Sb_{0.44}$ Avalanche Photodiode From Pure Electron Injection', *IEEE Photonics Technol. Lett.*, vol. 33, no. 20, pp. 1155–1158, Oct. 2021, doi: 10.1109/LPT.2021.3110123.

[18] J. D. Taylor-Mew, J. D. Petticrew, C. H. Tan, and J. S. Ng, 'Simulation of $Al_{0.85}Ga_{0.15}As_{0.56}Sb_{0.44}$ avalanche photodiodes', *Opt. Express*, vol. 30, no. 11, pp. 17946 – 17952, May 2022, doi: 10.1364/OE.458922.

[19] S. Xie X. Zhou, S. Zhang, D. J. Thomson, X. Chen, G. T. Reed, J. S. Ng, and C. H. Tan, 'InGaAs/AlGaAsSb avalanche photodiode with high gain-bandwidth product', *Opt. Express*, vol. 24, no. 21, pp. 24242 – 24247, Oct. 2016, doi: 10.1364/OE.24.024242.

[20] Y. Cao, T. Osman, E. Clarke, P. K. Patil, J. S. Ng, and C. H. Tan, 'A GaAsSb/AlGaAsSb Avalanche Photodiode With a Very Small Temperature Coefficient of Breakdown Voltage', *J. Light. Technol.*, vol. 40, no. 14, pp. 4709–4713, Jul. 2022, doi: 10.1109/JLT.2022.3167268.

[21] X. Collins, B. Sheridan, D. Price, Y. Cao, T. Blain, J. S. Ng, C. H. Tan, and B. White, 'Low-noise AlGaAsSb avalanche photodiodes for 1550 nm light detection', *Proc. SPIE*, vol. 12417, Mar. 2023, Art. no. 124170K. doi: 10.1117/12.2651669.

[22] B. Sheridan, X. Collins, J. D. Taylor-Mew, B. White, J. S. Ng, and C. H. Tan, 'An Extremely Low Noise-Equivalent Power Photoreceiver Using High-Gain InGaAs/AlGaAsSb APDs', *J. Light. Technol.*, Vol. 43, no. 2, pp. 741 – 746, Jan. 15, 2025, doi: 10.1109/JLT.2024.3447284.

[23] J. Taylor-Mew, X. Collins, J. D. Taylor-Mew, B. White, J. S. Ng, and C. H. Tan, 'Development of InGaAs/AlGaAsSb Geiger Mode Avalanche Photodiodes', *IEEE Trans. Electron Devices*, vol. 71, no. 3, pp. 1994–1998, Mar. 2024, doi: 10.1109/TED.2024.3354698.

[24] Y. Cao, T. Blain, J. D. Taylor-Mew, L. Li, J. S. Ng, and C. H. Tan, 'Extremely low excess noise avalanche photodiode with GaAsSb absorption region and AlGaAsSb avalanche region', *Appl. Phys. Lett.*, vol. 122, no. 5, Jan. 2023, Art. No. 051103, doi: 10.1063/5.0139495.

[25] S. Lee, X. Jin, H. Jung, H, Lewis, Y. Liu, B. Guo, S. H. Kodati, M. Schwartz, C. Grein, T. J. Ronningen, J. P. David, J. C. Campbell, and S. Krishna, 'High gain, low noise 1550 nm GaAsSb/AlGaAsSb avalanche photodiodes', *Optica*, vol. 10, no. 2, pp. 147 - 154, Feb. 2023, doi: 10.1364/OPTICA.476963.

[26] *Hamamatsu*, G1458-0020AA datasheet, 2019. Accessed: July 13, 2025. [Online]. Available: https://www.hamamatsu.com/content/dam/hamamatsu-photonics/sites/documents/99_SALES_LIBRARY/ssd/g14858 0020aa_kapd1068e.pdf.

[27] S. Abdullah, C. H. Tan, X. Zhou, S. Zhang, L. Pinel, and J. S. Ng, 'Investigation of temperature and temporal stability of AlGaAsSb avalanche photodiodes', *Opt. Express*, vol. 25, no. 26, pp. 33610 –33616, Dec. 2017, doi: 10.1364/OE.25.033610.

[28] L. Li *et al.*, Aug. 2025, "InGaAs/AlGaAsSb avalanche photodiodes with sub 100 fW/√Hz noise equivlent power at 22 to 52 °C," *ORDA Digital repository*, DOI: 10.15131/shef.data.26380576.

[29] *Phlux technology*, Aura noiseless InGaAs APD 200 μm datasheet, 2024. Accessed: July 13, 2025. [Online]. Available: https://phluxtechnology.com/assets/general/phlux -aura -datasheet -200um_2024 -01 -24 -130418_okts.pdf'.

[30] Stanford Research Systems, *SR 570 Low-Noise Current Preamplifier datasheet*, 2015. Accessed: July 13, 2025. [Online] Available: https://www.thinksrs.com/products/sr570.html.

[31] *Laser Components*, document Silicon Avalanche Photodiode SAE -Series (NIR -Enhanced) datasheet, 2023. Accessed: July 13, 2025. [Online]. Available:https://www.lasercomponents.com/fileadmin/user_upload/hom e/Datasheets/lc -apd/sae -series_nir -enhanced.pdf.

[32] *Hamamatsu*, Si APD (S14644 series) datasheet, 2021. Accessed: July 13, 2025. [Online]. Available: https://www.hamamatsu.com/content/dam/ham amatsu -photonics/sites/documents/99_SALES_LIBRARY/ssd/s14644_series_kapd1067e.pdf.

[33] A. Rouvie, D. Carpentier, N. Lagay, J. Decobert, F. Pommereau, and M. Achouche, 'High Gain × Bandwidth Product Over 140 -GHz Planar Junction AlInAs Avalanche Photodiodes', *IEEE Photonics Technol. Lett.*, vol. 20, no. 6, pp. 455 –457, Mar. 2008, doi: 10.1109/LPT.2008.918229.

[34] L. E. Tarof, J. Yu, T. Baird, R. Bruce, and D. G. Knight, 'Temperature measurements of separate absorption, grading, charge, and multiplication (SAGCM) InP/InGaAs avalanche photodiodes (APD's)', *IEEE Photonics Technol. Lett.*, vol. 5, no. 9, pp. 1044 –1046, Sep. 1993, doi: 10.1109/68.257186.

[35] J. S. L. Ong, J. S. Ng, A. B. Krysa, and J. P. R. David, 'Temperature dependence of avalanche multiplication and breakdown voltage in $Al_{0.52}In_{0.48}P$', *J. Appl. Phys.*, vol. 115, no. 6, p. 064507, Feb. 2014, doi: 10.1063/1.4865743.

[36] X. Zhou *et al.*, "Thin $Al_{1-x}Ga_xAs_{0.56}Sb_{0.44}$ diodes with extremely weak temperature dependence of avalanche breakdown', *R Soc Open Sci*, vol. 4, no. 5, May 2017, doi: 10.1098/rsos.170071"